Supplement of Atmos. Chem. Phys., 20, 4593–4605, 2020
https://doi.org/10.5194/acp-20-4593-2020-supplement

Atmospheric Chemistry and Physics
Open Access
EGU

Supplement of

The evolutionary behavior of chromophoric brown carbon during ozone aging of fine particles from biomass burning

Xingjun Fan et al.

Correspondence to: Jianzhong Song (songjzh@gig.ac.cn) and Xingjun Fan (fanxj@ahstu.edu.cn)

S1. Ozone aging reactor and operation

The ozone reactor consisted of oxygen and nitrogen sources, a gas flowmeter, an ozone generator, a humidity adjuster, a gas mixer and a principal reactor. All units were connected with polytetrafluoroethylene tubes. It is noted that all components in the reactor were wrapped with aluminum foil during oxidation to avoid any photolysis of O_3 and photo-chemical reactions. In this study, the O_3 was generated by the photolysis of dry air (99.9% purity) using an ultraviolet lamp (GPH212T5VH/4, Heraeus, German) with a wavelength of 185 nm. The O_3 was then diluted with a moisture flow generated by introducing pure N_2 (99.9% purity) into pure water. The RH and temperature in principal reactor were monitored with a digital thermo-hygrograph (TH20R-EX, Huahanwei, Shenzhen, China), and the O_3 was measured using an ozone detector (XLA-BX-03, Pulitong, Shenzhen, China).

According to previous studies, the O_3 oxidation simulation experiments of carbonaceous compounds have been conducted under different O_3 concentration (20 ppb – 12,200 ppm) (Baduel et al., 2011; D'Anna et al., 2009; Pillar et al., 2014, 2017). For example, low O_3 concentrations (20 ppb - 6 ppm) had been used for oxidizing the thin films of humic matter (Baduel et al., 2011; D'Anna et al., 2009) and oxy-aromatics (i.e. catechol and its substituted ones) (Pillar et al., 2014, 2017), in which the changes of the early aging mechanism occurred in air-particle interface had been explored. In addition, to explore the changes of physicochemical properties of particulate samples from combustion process, or to investigate the optical properties of newly formed light absorbing organic compounds during O_3 aging process, a relatively high O_3 concentrations (20 ppm-12,200 ppm) were commonly used in the simulation experiments (Li et al., 2013, 2015; Decesari et al., 2002; Gallimore et al., 2011; Pillar et al., 2015; Zhu et al., 2019). Importantly, some studies have revealed that the oxidation mechanism at higher O_3 concentration is similar to that done at much lower O_3 concentration (Pillar et al., 2015; Gallimore et al., 2011). In this study, BB smoke samples are very complex, which comprised not only the low molecular weight organic compounds (i.e. lignin-derived aromatics) and macromolecular organic matter (e.g. BrC), but also soot materials (Fan et al., 2018; Hong et al., 2017; Huo et al., 2018; Schmidl et al, 2011). To investigate the evolutionary behavior of chromophoric BrC compounds during O_3 aging of the complex BB smoke samples, thus a relative high O_3 concentration of 70 ppm was used in this study (Decesari et al., 2002; Li et al., 2013, 2015; Zhu et al., 2019). In addition, a moderate RH (~40%) and room temperature (25 ºC) were maintained in the aging process and the air and N_2 flow rates were both set at ~0.5 L/min.

In this study, the O_3 exposure amount for 1 h in reactor were ~1.7×10^{15} molec cm^{-3} h. For a highly O_3 polluted (~120 ppb) area (Chen et al., 2020), 24 h-average atmospheric O_3 exposure amount were ~7.1×10^{13} molec cm^{-3} h. In this case, the

oxidation for 24 h in our reactor was greatly higher than those exposure at polluted atmosphere during their lifetime (up to 14 days) in atmosphere. However, this calculation was obtained based on an assumption that smoke particles were suspended in reactor. In fact, our smoke samples were highly condensed and coagulated, so the exposure area of particles were greatly reduced. As a result, the equivalent day for O_3 oxidation should be highly shortened. Moreover, our results showed many similar oxidation behaviors of organic chromophores to those of atmospheric humic matter and BB-derived oxy-aromatics under low O_3 concentration (20 ppb- 6 ppm) (Baduel et al., 2011; D'Anna et al., 2009; Pillar et al., 2014, 2017). Therefore, we believed that the evolutionary behaviors of BB-BrC revealed in this study might resemble those occurred under relatively low O_3 concentration during their lifetime in atmospheric environment.

S2. Control experiments

In this study, two types of control experiment were conducted. The first was a blank control, which was conducted by using blank filters whose treatments were the same as that used to aging of the fine smoke particles. The other was a smoke-particle control experiment, which was conducted under similar oxidation conditions but without O_3 introduction.

For both control experiments, the filter samples were uniformly spread on the glass garden, and then put into the ozone reactor. For the blank filters, the temperature, humidity and O_3 concentration in the reactor were set to 25 °C, 40%, and 70 ppm, respectively. For the smoke-particle filter control experiment, no ozone was introduced into the reactor. After 24 h of aging, three pieces of blank filter and smoke filter for each biomass burning (BB) sample were taken out. Then, extraction and filtration of the water soluble BrC were carried out following the method introduced in Section 2.3. Finally, the TOC, UV-vis spectra and fluorescence spectra of the fresh and aged BrC were obtained.

The TOC content of the blank filter extracts were near the detection limits of our instruments, and the light absorption and fluorescence intensity over all wavelengths were about zero. These results suggest that no organic chromophores had formed during the O_3 aging of the blank filters. Next, the TOC content, UV-vis spectra and EEM spectra of the extracts of the fresh and 24-h-aged smoke filter samples without O_3 exposure also did not show any observable differences. For example, it is obvious from inspection of the UV-vis spectra (Figure S1) and the EEM spectra (Figure S2) of the controlled BrC that they do not exhibit any significant differences in their spectral patterns and intensities compared to the initial ones for the three types of BB smoke samples.

S3. Optical indices

In this study, the specific UV absorbance at 254 nm ($SUVA_{254}$), the absorption Angstrom exponent (AAE), the mass absorption efficiency (MAE_{365}) and the humification index (HIX) were calculated to investigate the effects of ozone aging on the optical properties of water-soluble BrC in the BB smoke samples.

$SUVA_{254}$ was calculated as UV254/(b × c), where b is the cell path length (0.01 m) and c is the BrC content (mgC/L). $SUVA_{254}$ has been reported to correlate with the aromaticity of BrC (Fan et al., 2016).

AAE is indicative of the wavelength dependence of the light absorption of BrC (Fan et al., 2016;Cheng et al., 2016;Park and Yu, 2016;Huo et al., 2018), which were investigated using the following equation:

$$A_\lambda = K\,\lambda^{-AAE} \quad (1)$$

where A_λ is the UV absorbance at a given wavelength λ, and K is a constant. In the present work, the AAE values were fitted within the range of 330–400 nm.

MAE_{365} is another absorption index that characterizes the light absorption ability of BrC (Chen et al., 2016a;Fan et al., 2016;Huo et al., 2018;Park and Yu, 2016), which was determined using the following equation:

$$MAE_{365} = \frac{A_\lambda}{c \cdot l} \cdot \ln(10) \quad (2)$$

where c is the TOC concentration of BrC (μg/mL) and l is the optical path length (0.01 m).

HIX was measured by dividing the area of the fluorescence intensity between 435 and 480 nm by that between 300 and 345 nm, given as Ex = 254 nm (Qin et al., 2018). HIX reflects the degree of humification and the complexity of the BrC.

S4. Observations of the absorption and fluorescence spectra of BrC

The variations of the absorption and fluorescence spectra of BrC as a function of O_3 aging time are shown in Figure S3 and Figure S4, respectively. In general, the absorption and fluorescence spectra patterns of both the fresh and O_3-aged BB-BrC are similar to those of the WSOC and HULIS fractions in ambient aerosols and rainwater (Santos et al., 2012;Duarte et al., 2004;Fan et al., 2012), suggesting that both fresh BB emission and aged emission are important, atmospherically relevant sources of BrC.

As shown in Figure S3 and Figure S4, the intensity and shape of the BB-BrC spectra exhibited some changes during the O_3 aging process. It is obvious that the absorption intensity of the BB-BrC gradually decreases with an extension of the O_3 aging time, indicating that O_3 aging can lead to the decomposition of chromophores in BB-BrC. The decrease of chromophores is strongly consistent with the results of the

photo-chemical aging of BB-BrC previously reported both in laboratory and field studies, in which noticeable photobleaching was frequently investigated (Forrister et al., 2015;Lee et al., 2014;Zhao et al., 2015). In addition, the shapes of the absorption spectra of BB-BrC also changed due to O_3 aging. For example, an apparent shoulder can be observed in the UV-vis spectra of the RS- and CS- BrC, which shifts from ~254 nm for fresh BrC and to ~280 nm for oxidized BrC (Figure S3). This red shift suggests that poly-conjugated and polymeric structures have formed, but they gradually decomposed with an extension of the O_3 oxidation time. For the PW-BrC, the apparent shoulder at ~280 nm for fresh BrC was absent for the oxidized BrC, suggesting the decomposition of weakly poly-conjugated chromophores.

The fluorescence intensities of the BB-BrC also presented gradual decreases during the O_3 aging process, indicating the decomposition of fluorophores. After 24 h of O_3 aging, the reduction of fluorescent intensity at 290 nm for the BB-BrC are in the order of PW (87%) > CS (71%) > RS (50%). Moreover, the shapes of the synchronous fluorescence spectra for the BB-BrC also changed significantly, which showed a sharp decrease of the peak at ~290 nm and a slight decrease of the peak at ~325 nm (Figure S4). These two peaks are mainly located in protein-like and fulvic-like fluorescent regions, respectively (Hur and Lee, 2014;Chen et al., 2015). Therefore, the ratio of the fluorescence intensity of the peak at 290 nm to that of the peak at 325 nm (fl290/fl325) indicates the relative distribution of the protein-like and fulvic-like fluorophores in BrC. In the present study, the fl290/fl325 ratios changed from 1.1 to 0.8, 2.0 to 1.1, and 2.2 to 1.3 for the RS-, CS-, and PW- BrC, respectively. These results suggest that the protein-like fluorophore is labile to decompose during O_3 aging, which was also verified by the EEM-PARAFAC analysis (Section 3.3).

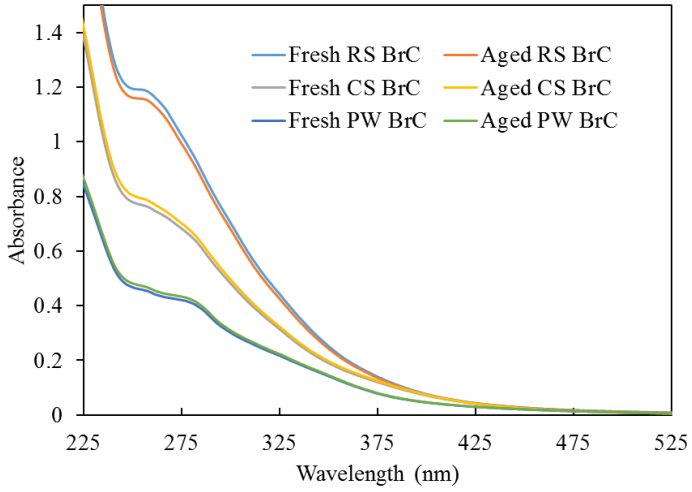

Figure S1. The UV-vis spectra of the RS-, CS- and PW- BrC from the control experiments. Note: fresh BrC represent water extracts in fresh smoke particles, aged BrC herein represents water extracts in smoke particles which have exposed in the reactor via similar conditions as the formal experiment but without O_3 aging for 24 h.

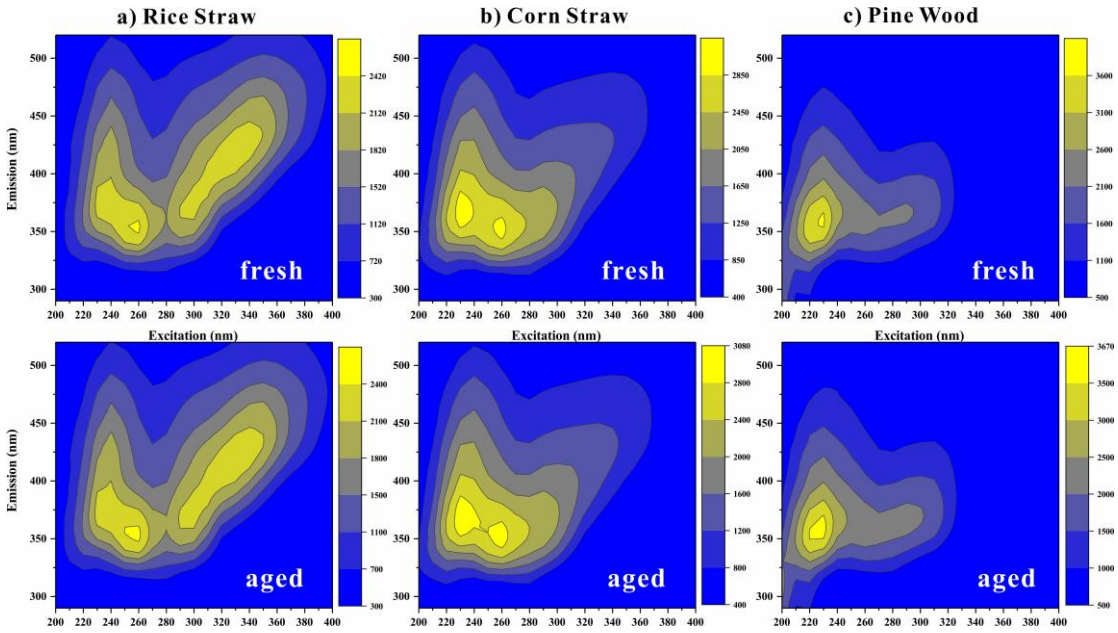

Figure S2. The EEM spectra of the RS-, CS- and PW- BrC from the control experiments. Note: fresh BrC represent water extracts in fresh smoke particles, aged BrC herein represents water extracts in smoke particles which have exposed in the reactor via similar conditions as the formal experiment but without O_3 aging for 24 h.

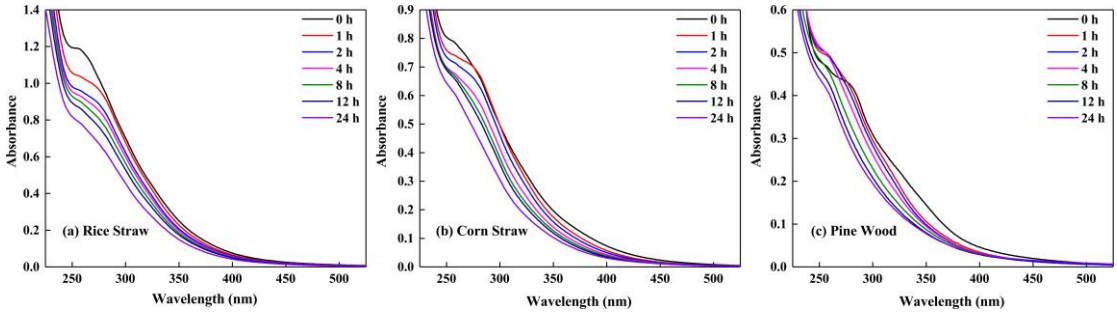

Figure S3. Dynamic variations of the UV-vis spectra of BrC in (a) RS, (b) CS and (c) PW smoke particles during O_3 aging.

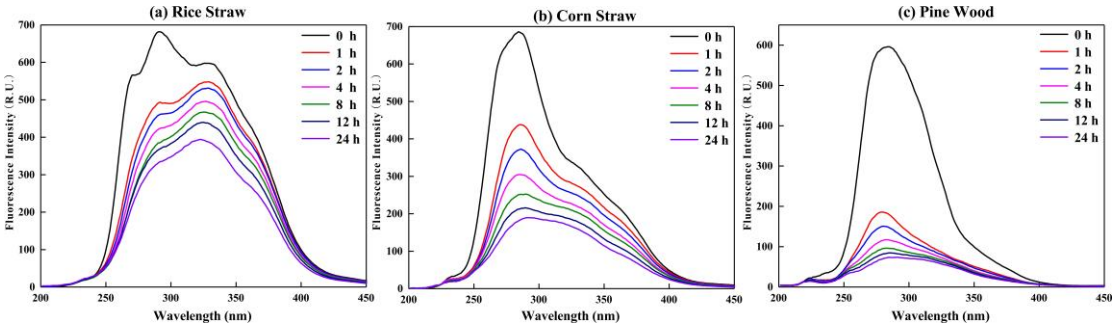

Figure S4. Dynamic variations for the synchronous fluorescence spectra of BrC in (a) RS, (b) CS and (c) PW smoke particles during O_3 aging.

Table S1. Characteristics of the four components identified with EEM-PARAFAC in this study, which are compared with previously identified components in the literature.

Components	Ex/Em (nm)	Fluorescent compounds	Descriptions and assignments	Sources and references
C1	250(300,340)/450	HULIS-1	Long-wavelength humic-like chromophores with high molecular weight	Urban organic aerosol extracts (Chen et al., 2016a), urban, forest and marine aerosols WSOM (Chen et al., 2016b), crop straw combustion emitted HULIS (Huo et al., 2018), compost-derived DOM (Huang et al., 2018), agricultural soil DOM (Gao et al., 2017), biochar DOM (Jamieson et al., 2014)
C2	240(320)/390	HULIS-2	Short-wavelength humic-like chromophores with less oxygenated chromophores	Urban organic aerosol extracts (Chen et al., 2016a), urban, forest and marine Aerosols WSOM (Chen et al., 2016b), compost-derived DOM (Huang et al., 2018), biochar DOM (Jamieson et al., 2014)
C3	270(230)/355	PLOM	Protein-like organic matters, mainly as tryptophan-like and even non-nitrogen-containing chromophores	Urban organic aerosol extracts (Chen et al., 2016a), urban, forest and marine Aerosols WSOM (Chen et al., 2016b), crop straw combustion emitted HULIS (Huo et al., 2018), rice-straw-derived DOM (Huang et al., 2018),
C4	230(280)/415	HULIS-3	Short-wavelength humic-like chromophores with highly oxygenated chromophores	Urban organic aerosol extracts (Chen et al., 2016a), urban, forest and marine Aerosols WSOM (Chen et al., 2016b), crop straw combustion emitted HULIS (Huo et al., 2018), rice-straw-derived DOM (Huang et al., 2018)

Table S2. Sign of each cross-peak in the synchronous and asynchronous maps (shown in brackets) from the results of the 2D-SF-COS for (a) RS-, (b) CS- and (c) PW- BrC.

(a) Rice straw BrC

Position (nm)	Assignment	Sign		
		267	289	333
267	Protein-like	+	+(+)	+(+)
289	Protein-like		+	+(+)
333	Fulvic-like			+

(b) Corn straw BrC

Position (nm)	Assignment	Sign		
		263	284	340
263	Protein-like	+	+(+)	+(+)
284	Protein-like		+	+(+)
340	Fulvic-like			+

(c) Pine wood BrC

Position (nm)	Assignment	Sign		
		276	309	358
276	Protein-like	+	+(-)	+(+)
309	Fulvic-like		+	+(+)
358	Fulvic-like			+

Table S3. Sign of each cross-peak in the synchronous and asynchronous maps (shown in brackets) from the results of the 2D-FTIR-COS for (a) RS-, (b) CS- and (c) PW- BrC.

(a) Rice straw BrC

Position (cm^{-1})	Assignment	Sign[a]			
		1725	1580	1515	1224
1725	Carboxyl $\nu_{C=O}$ (carbonyl C=O)	+	-(-)	-(-)	+(-)
1580	C=O bonded to an aromatic ring (ν_{COO^-})		+	+(+)	-(+)
1515	Lignin skeletal (aromatic) $\nu_{C=C}$			+	-(+)
1224	Phenolic ν_{C-O}, δ_{O-H}				+

(b) Corn straw BrC

Position (cm^{-1})	Assignment	Sign				
		1726	1639	1515	1400	1211
1726	Carboxyl $\nu_{C=O,}$ ν_{C-O}	+	+(+)	-(-)	+(-)	+(-)
1639	Aromatic ketone $\nu_{C=O}$		+	-(-)	+(-)	+(-)
1515	Lignin skeletal (aromatic) $\nu_{C=C}$			+	/(+)	/(+)
1400	Phenolic ν_{C-O}, δ_{O-H}				+	+(/)
1211	Phenolic ν_{C-O}, δ_{O-H}					+

(c) Pine wood BrC

Position (cm^{-1})	Assignment	Sign				
		1725	1630	1585	1515	1318
1725	Carboxylic $\nu_{C=O}$	+	+(-)	-(-)	-(-)	+(+)
1630	Aromatic ketone $\nu_{C=O}$		+	-(-)	-(-)	+(+)
1585	Aromatic ν_{COO^-}			+	-(-)	+(+)
1515	Lignin skeletal (aromatic) $\nu_{C=C}$				+	/(/)
1318	Aliphatic ν_{C-H}, ν_{C-O}					+

[a] Signs were obtained in the upper-left corner of the maps shown in Figure 4: +, positive; -, negative

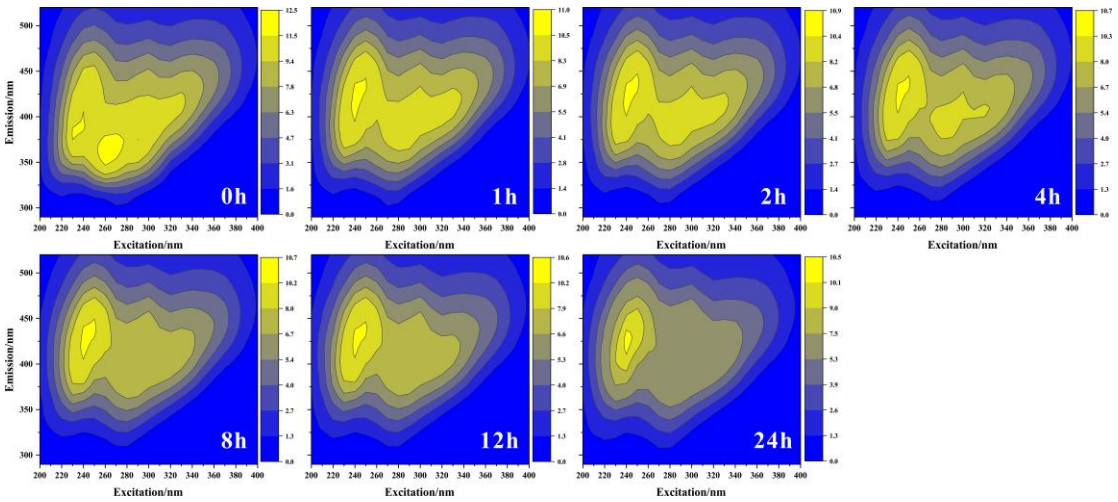

Figure S5. Variations of the EEM spectra of BrC in RS-burning smoke particles during O_3 aging.

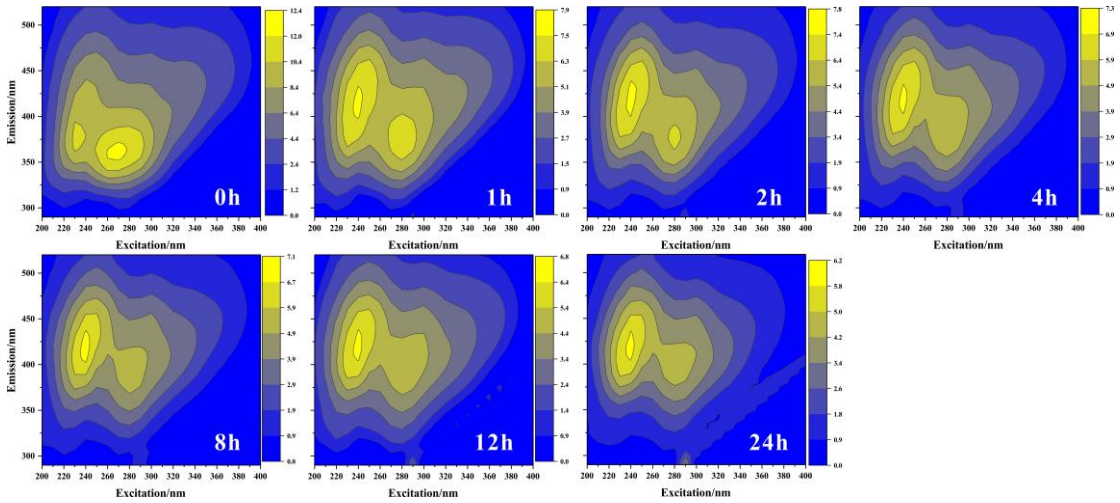

Figure S6. Variations of the EEM spectra of BrC in CS-burning smoke particles during O_3 aging.

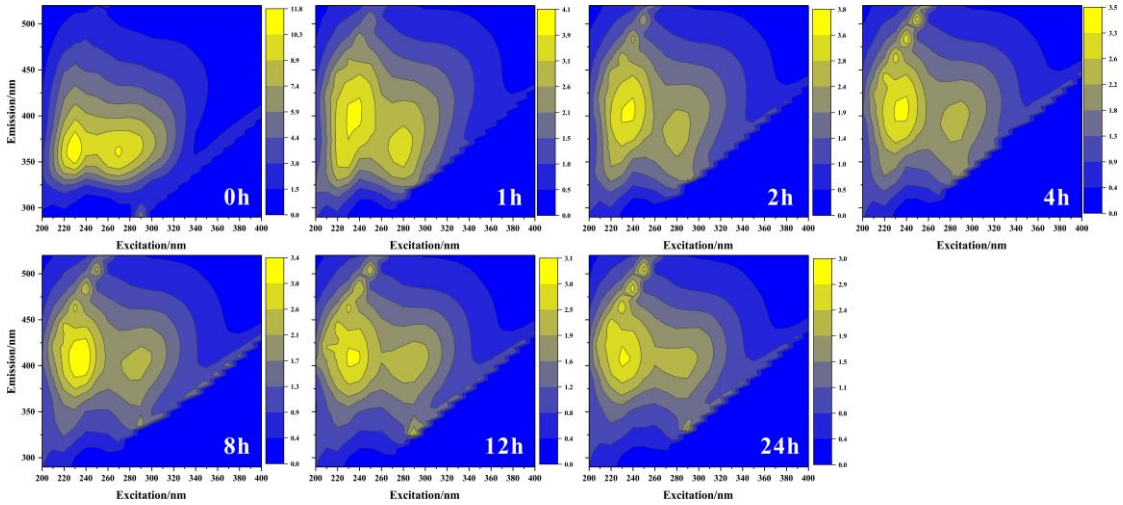

Figure S7. Variations of the EEM spectra of BrC in PW-burning smoke particles during O_3 aging.

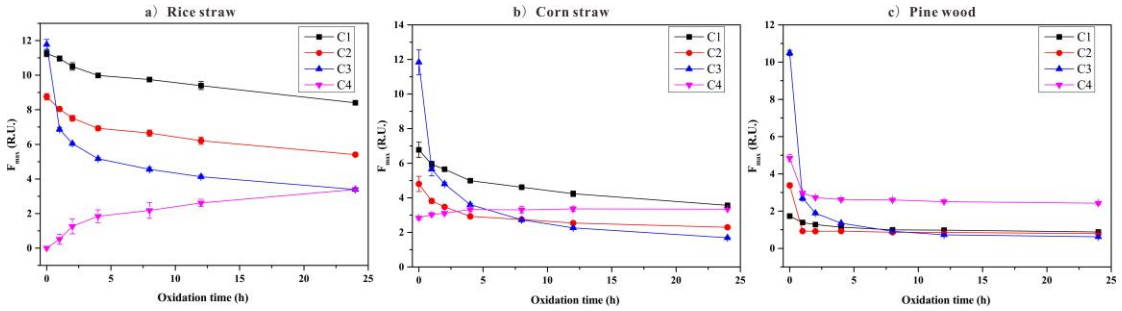

Figure S8. Changes in fluorescence intensity (R.U.) of the PARAFAC-derived fluorescent components within BrC extracted from the (a) RS-, (b) CS- and (c) PW- burning smoke particles during O_3 aging.

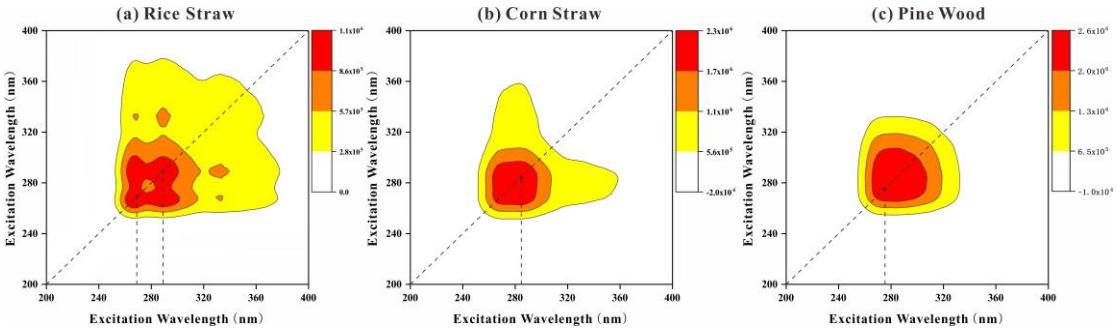

Figure S9. Synchronous 2D correlation fluorescence spectra of BrC in the (a) RS-, (b) CS- and (c) PW- burning smoke particles during O_3 aging.

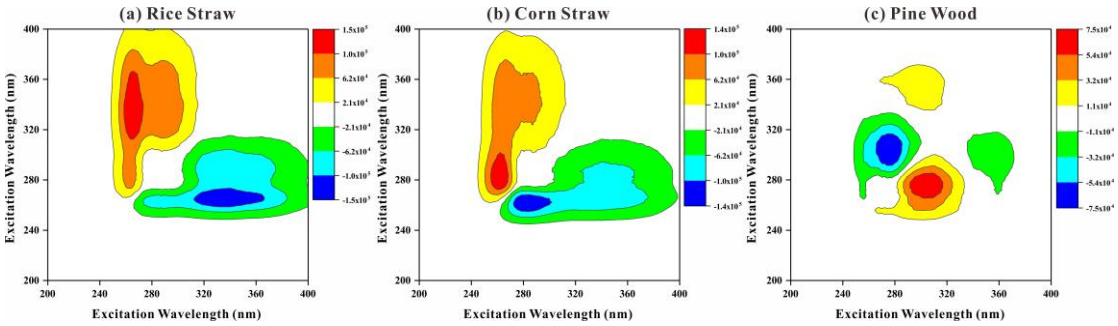

Figure S10. Asynchronous 2D correlation fluorescence spectra of BrC in the (a) RS-, (b) CS- and (c) PW- burning smoke particles during O_3 aging.

References

Baduel, C., Monge, M. E., Voisin, D., Jaffrezo, J. L., George, C., Haddad, I. E., Marchand, N., and D'Anna, B.: Oxidation of atmospheric humic like substances by ozone: a kinetic and structural analysis approach, Environ. Sci. Technol., 45, 5238-5244, https://doi.org/10.1021/es200587z, 2011.

Chen, Q., Ikemori, F., and Mochida, M.: Light Absorption and Excitation-Emission Fluorescence of Urban Organic Aerosol Components and Their Relationship to Chemical Structure, Environ. Sci. Technol., 50, 10859-10868, https://doi.org/10.1021/acs.est.6b02541, 2016a.

Chen, Q., Miyazaki, Y., Kawamura, K., Matsumoto, K., Coburn, S., Volkamer, R., Iwamoto, Y., Kagami, S., Deng, Y., Ogawa, S., Ramasamy, S., Kato, S., Ida, A., Kajii, Y., and Mochida, M.: Characterization of Chromophoric Water-Soluble Organic Matter in Urban, Forest, and Marine Aerosols by HR-ToF-AMS Analysis and Excitation-Emission Matrix Spectroscopy, Environ. Sci. Technol., 50, 10351-10360, https://doi.org/10.1021/acs.est.6b01643, 2016b.

Chen, W., Habibul, N., Liu, X. Y., Sheng, G. P., and Yu, H. Q.: FTIR and synchronous fluorescence heterospectral two-dimensional correlation analyses on the binding characteristics of copper onto dissolved organic matter, Environ. Sci. Technol., 49, 2052-2058, https://doi.org/10.1021/es5049495, 2015.

Cheng, Y., He, K.-b., Du, Z.-y., Engling, G., Liu, J.-m., Ma, Y.-l., Zheng, M., and Weber, R. J.: The characteristics of brown carbon aerosol during winter in Beijing, Atmos. Environ., 127, 355-364, http://dx.doi.org/10.1016/j.atmosenv.2015.12.035, 2016.

Chen, Z.; Li, R.; Chen, D.; Zhuang, Y.; Gao, B.; Yang, L.; Li, M.: Understanding the causal influence of major meteorological factors on ground ozone concentrations across China. Journal of Cleaner Production, 242, 118498, https://doi.org/10.1016/j.jclepro.2019.118498, 2020.

D'Anna, B., Jammoul, A., George, C., Stemmler, K., Fahrni, S., Ammann, M., and Wisthaler, A.: Light-induced ozone depletion by humic acid films and submicron aerosol particles, Journal of Geophysical Research, 114, https://doi.org/10.1029/2008jd011237, 2009.

Decesari, S., Facchini, M. C., Matta, E., Mircea, M., Fuzzi, S., Chughtai, A. R., and Smith, D. M.: Water soluble organic compounds formed by oxidation of soot, Atmos. Environ., 36, 1827-1832, 2002.

Duarte, R. M. B. O., Pio, C. A., and Duarte, A. C.: Synchronous scan and excitation-emission matrix fluorescence spectroscopy of water-soluble organic compounds in atmospheric aerosols, J. Atmos. Chem., 48, 157-171, 2004.

Fan, X., Wei, S., Zhu, M., Song, J., and Peng, P.: Comprehensive characterization of humic-like substances in smoke PM2.5 emitted from the combustion of biomass materials and fossil fuels, Atmos. Chem. Phys., 16, 13321-13340, https://doi.org/10.5194/acp-16-13321-2016, 2016.

Fan, X. J., Song, J. Z., and Peng, P. A.: Comparison of isolation and quantification methods to measure humic-like substances (HULIS) in atmospheric particles, Atmos. Environ., 60,

366-374, https://doi.org/10.1016/j.atmosenv.2012.06.063, 2012.

Fan, X., Li, M., Cao, T., Cheng, C., Li, F., Xie, Y., Wei, S., Song, J., and Peng, P. a.: Optical properties and oxidative potential of water- and alkaline-soluble brown carbon in smoke particles emitted from laboratory simulated biomass burning, Atmos. Environ., 194, 48-57, https://doi.org/10.1016/j.atmosenv.2018.09.025, 2018.

Forrister, H., Liu, J., Scheuer, E., Dibb, J., Ziemba, L., Thornhill, K. L., Anderson, B., Diskin, G., Perring, A. E., Schwarz, J. P., Campuzano-Jost, P., Day, D. A., Palm, B. B., Jimenez, J. L., Nenes, A., and Weber, R. J.: Evolution of brown carbon in wildfire plumes, Geophysical Research Letters, 42, 4623-4630, https://doi.org/10.1002/2015gl063897, 2015.

Gao, J., Liang, C., Shen, G., Lv, J., and Wu, H.: Spectral characteristics of dissolved organic matter in various agricultural soils throughout China, Chemosphere, 176, 108-116, https://doi.org/10.1016/j.chemosphere.2017.02.104, 2017.

Hong, L.; Liu, G.; Zhou, L.; Li, J.; Xu, H.; Wu, D.: Emission of organic carbon, elemental carbon and water-soluble ions from crop straw burning under flaming and smoldering conditions. Particuology, 31, 181-190, https://doi.org/10.1016/j.partic.2016.09.002, 2017.

Huang, M., Li, Z., Huang, B., Luo, N., Zhang, Q., Zhai, X., and Zeng, G.: Investigating binding characteristics of cadmium and copper to DOM derived from compost and rice straw using EEM-PARAFAC combined with two-dimensional FTIR correlation analyses, J Hazard Mater, 344, 539-548, https://doi.org/10.1016/j.jhazmat.2017.10.022, 2018.

Huo, Y., Li, M., Jiang, M., and Qi, W.: Light absorption properties of HULIS in primary particulate matter produced by crop straw combustion under different moisture contents and stacking modes, Atmos. Environ., 191, 490-499, https://doi.org/10.1016/j.atmosenv.2018.08.038, 2018.

Hur, J., and Lee, B.-M.: Characterization of copper binding properties of extracellular polymeric substances using a fluorescence quenching approach combining two-dimensional correlation spectroscopy, Journal of Molecular Structure, 1069, 79-84, https://doi.org/10.1016/j.molstruc.2013.11.056, 2014.

Jamieson, T., Sager, E., and Guéguen, C.: Characterization of biochar-derived dissolved organic matter using UV–visible absorption and excitation–emission fluorescence spectroscopies, Chemosphere, 103, 197-204, http://dx.doi.org/10.1016/j.chemosphere.2013.11.066, 2014.

Lee, H. J., Aiona, P. K., Laskin, A., Laskin, J., and Nizkorodov, S. A.: Effect of Solar Radiation on the Optical Properties and Molecular Composition of Laboratory Proxies of Atmospheric Brown Carbon, Environ. Sci. Technol., 48, 10217-10226, https://doi.org/10.1021/es502515r, 2014.

Li, Q., Shang, J., and Zhu, T.: Physicochemical characteristics and toxic effects of ozone-oxidized black carbon particles, Atmos. Environ., 81, 68-75, https://doi.org/10.1016/j.atmosenv.2013.08.043, 2013.

Li, Q., Shang, J., Liu, J., Xu, W., Feng, X., Li, R., and Zhu, T.: Physicochemical characteristics, oxidative capacities and cytotoxicities of sulfate-coated, 1,4-NQ-coated and ozone-aged

black carbon particles, Atmos. Res., 153, 535-542, https://doi.org/10.1016/j.atmosres.2014.10.005, 2015.

Park, S. S., and Yu, J.: Chemical and light absorption properties of humic-like substances from biomass burning emissions under controlled combustion experiments, Atmos. Environ., 136, 114-122, https://doi.org/10.1016/j.atmosenv.2016.04.022, 2016.

Pillar, E. A.; Camm, R. C.; Guzman, M. I.: Catechol Oxidation by Ozone and Hydroxyl Radicals at the Air–Water Interface. Environmental Science & Technology, 48, (24), 14352-14360, https://doi.org/10.1021/es504094x, 2014.

Pillar, E. A.; Guzman, M. I.: Oxidation of Substituted Catechols at the Air-Water Interface: Production of Carboxylic Acids, Quinones, and Polyphenols. Environ Sci Technol, 51, (9), 4951-4959, https://doi.org/10.1021/acs.est.7b00232, 2017.

Qin, J., Zhang, L., Zhou, X., Duan, J., Mu, S., Xiao, K., Hu, J., and Tan, J.: Fluorescence fingerprinting properties for exploring water-soluble organic compounds in PM 2.5 in an industrial city of northwest China, Atmos. Environ., 184, 203-211, https://doi.org/10.1016/j.atmosenv.2018.04.049, 2018.

Santos, P. S. M., Santos, E. B. H., and Duarte, A. C.: First spectroscopic study on the structural features of dissolved organic matter isolated from rainwater in different seasons, Sci. Total Environ., 426, 172-179, https://doi.org/10.1016/j.scitotenv.2012.03.023, 2012.

Schmidl, C.; Luisser, M.; Padouvas, E.; Lasselsberger, L.; Rzaca, M.; Ramirez-Santa Cruz, C.; Handler, M.; Peng, G.; Bauer, H.; Puxbaum, H.: Particulate and gaseous emissions from manually and automatically fired small scale combustion systems. Atmospheric Environment, 45, (39), 7443-7454, https://doi.org/10.1016/j.atmosenv.2011.05.006, 2011.

Zhao, R., Lee, A. K. Y., Huang, L., Li, X., Yang, F., and Abbatt, J. P. D.: Photochemical processing of aqueous atmospheric brown carbon, Atmos. Chem. Phys., 15, 6087-6100, https://doi.org/10.5194/acp-15-6087-2015, 2015.

Zhu, J., Chen, Y., Shang, J., and Zhu, T.: Effects of air/fuel ratio and ozone aging on physicochemical properties and oxidative potential of soot particles, Chemosphere, 220, 883-891, https://doi.org/10.1016/j.chemosphere.2018.12.107, 2019.